Chapter 3

Using strong gravitational lensing to probe the post reionization H I power spectrum

* Strong lensing phenomena is described as the phenomena of bending of light through large masses in the universe similar to the bending of light in the optical context. There are large mass regions inside the Universe that works as natural telescopes. This lens can cause the magnification of the signal behind it. Here we are considering galaxy clusters as gravitational lenses. In this chapter, we will study the effect of strong gravitational lens on the 21 cm power spectrum from post-reionization era with four different lens models.

*A part of the work presented in this chapter is originally published in the paper titled " Using strong gravitational lensing to probe the post reionization HI power spectrum" by (Arora and Dutta, 2020)

3.1 Formalism

3.1.1 Visibility function of lensed H I emission

Specific intensity of H I emission at the observer $I_{obs}(\vec{\theta}, z_s, z_L)$, originating from a direction $\vec{\theta}$ in the sky (with respect to the centre of the field of view of observation) at the redshift z_s and modified by a strong gravitational lens at the redshift z_L can be written as

$$I_{obs}(\vec{\theta}, z_s, z_L) = \int d\vec{\theta}' \left[I_0 + \delta I(\vec{\theta}', z_s) \right] G_L(\vec{\theta} - \vec{\theta}', z_s, z_L), \tag{3.1}$$

where $G_L(\vec{\theta}, z_s, z_L)$ is the point spread function of the gravitational lens. Redshift dependence on the specific intensity at the observer arises from (i) the redshifted frequency of the 21 cm emission and (ii) the point spread function of the gravitational lens G_L. The point spread function of the gravitational lens also depends on the angular direction in the sky. We shall discuss these dependencies in detail in a later section. The observed visibility by radio interferometers of such lensed H I emission can be written as

$$V(\vec{U}, z_s, z_L) = \int d\vec{\theta}' \int d\vec{\theta}\, \delta I(\vec{\theta}', z_s) A(\vec{\theta}, z_s) G_L(\vec{\theta} - \vec{\theta}', z_s, z_L) \exp(-i2\pi \vec{U}.\vec{\theta}). \tag{3.2}$$

We have assumed here that the angular extent of the gravitational lens is small and the flat sky approximation is valid. Since the interferometers do not observe at zero baselines, the first term in the integral of eqn (3.1) is not measured. The antenna beam pattern $A(\vec{\theta})$ of the telescope depends on the source redshift through the observing frequency and is related to the aperture function $\tilde{a}(\vec{U})$ as

$$A(\vec{\theta}) = \int d\vec{U}\, \tilde{a}(\vec{U})\, e^{i2\pi \vec{U}.\vec{\theta}}. \tag{3.3}$$

Here, we investigate the effect of strong lensing on intensity mapping of the redshifted 21 cm emission from the neutral hydrogen. 21 cm intensity mapping is discussed in Bharadwaj et al. (2001) and Bharadwaj and Ali (2005). The brightness temperature fluctuation in 21 cm emission is related to the 21 cm radiation efficiency $\eta_{HI}(\vec{x})$ as (Bharadwaj and Ali, 2005)

$$\delta I(\vec{\theta}, z_s) = \frac{\partial B}{\partial T} \bar{T}(z_s) \eta_{HI}(\vec{x}, z_s) \tag{3.4}$$

where B is the Planck's function and $\bar{T}(z_s)$ can be calculated for a background cosmology as

$$\bar{T}(z_s) = 4.0mK(1+z_s)^2 \left(\frac{\Omega_b h^2}{0.02}\right) \left(\frac{0.7}{h}\right) \left(\frac{H_0}{H(z_s)}\right). \tag{3.5}$$

We define the lensing sampling function $S_L(\vec{U}, z_s, z_L)$ as

$$G_L(\vec{\theta}, z_s, z_L) = \int d\vec{U} S_L(\vec{U}, z_s, z_L) e^{i2\pi \vec{U}.\vec{\theta}}. \tag{3.6}$$

The observed (lensed) visibility can be written as

$$V(\vec{U}', z_s, z_L) = \bar{T}(z_s) \frac{\partial B}{\partial T} \int \frac{d\vec{k}}{(2\pi)^3} \eta_{HI}(\vec{k}) S_L \left(\frac{r_\nu \vec{k}_\perp}{2\pi}, z_s, z_L\right) \tilde{a}\left(\vec{U} - \frac{r_\nu \vec{k}_\perp}{2\pi}\right) e^{ik_\parallel r_\nu}, \tag{3.7}$$

where the quantity $\tilde{\eta}_{HI}(\vec{k}, z_s)$ gives the 21 cm radiation efficiency in the Fourier space as

$$\eta_{HI}(\vec{x}, z_s) = \int \frac{d\vec{k}}{(2\pi)^3} \tilde{\eta}_{HI}(\vec{k}, z_s) e^{i\vec{k}.\vec{x}}. \tag{3.8}$$

We have used $\vec{k}.\vec{x} = r_\nu[k_\parallel + \vec{k}_\perp.\vec{\theta}]$ with $\parallel$ denotes the component of the vector $\vec{k}$ along the line of sight of observation and $\perp$ denotes the components in the plane of the sky, $\vec{x}$ represents the comoving position vector. The quantity r_ν denotes the comoving distance to the redshift, where for the observing frequency ν and rest frequency of 21 cm emission ν_0, $z_s = \nu_0/\nu - 1$.

3.1.2 Power spectrum for the lensed H I emission

Here, we use the observed visibility correlation to estimate 21 cm power spectrum from redshift z_s modified by an intervening strong gravitational lens at redshift z_L. We denote the visibility correlation with lensing as V_{2L}, where

$$V_{2L}(\vec{U},\vec{U'},\nu,\Delta\nu) = C'(z)\int \frac{dk_\parallel d\vec{k}_\perp}{(2\pi)^3} e^{-ik_\parallel r'_\nu \Delta\nu} S_L^*\left(\frac{r_\nu \vec{k}_\perp}{2\pi}, z_s, z_L\right) S_L\left(\frac{r_{\nu_1}\vec{k}_\perp}{2\pi}, z_s, z_L\right)$$
$$\tilde{a}^*(\vec{U} - \frac{r_\nu \vec{k}_\perp}{2\pi})\tilde{a}\left(\vec{U'} - \frac{r_{\nu_1}\vec{k}_\perp}{2\pi}\right) P_{HI}(\vec{k}).$$

Here $\nu_1 = \nu + \Delta\nu$, $C'(z) = \left[\bar{T}(z_s)\frac{\partial B}{\partial T}\right]^2$, r_{ν_1} is the comoving distance at frequency $\nu + \Delta\nu$

$$r_{\nu_1} = r(\nu) + \frac{\partial r_\nu}{\partial \nu}\Delta\nu = r_\nu + r'_\nu \Delta\nu. \tag{3.9}$$

The aperture function of a telescope depends on the dipole pattern as well as the antenna dimensions. For this calculation, we assume $A(\vec{\theta}) = \exp(-\frac{\theta^2}{\theta_0^2})$, where the parameter θ_0 quantifies the field of view of the observation. The functions S_L and $\tilde{a}$ depends weakly on r_ν, where we assume $S_L(r_{\nu_1}\vec{k}_\perp/2\pi, z_s, z_L) = S_L(r_\nu \vec{k}_\perp/2\pi, z_s, z_L)$ and $\tilde{a}(\vec{U'} - r_{\nu_1}\vec{k}_\perp/2\pi) = \tilde{a}(\vec{U'} - r_\nu \vec{k}_\perp/2\pi)$. For $k_\perp >> \frac{2}{r_\nu \theta_0}$ the visibility correlation can be written as

$$V_{2L}(\vec{U},\vec{U'},\nu,\Delta\nu) = \quad C(z) \mid S_L(\vec{U}, z_s, z_L) \mid^2 \int dk_\parallel e^{-ik_\parallel r'_\nu \Delta\nu}$$
$$\exp\left(-\frac{|\frac{2\pi}{r_\nu}(\vec{U}-\vec{U'}|^2}{(\frac{2}{r_\nu\theta_0})^2}\right) P_{HI}(\sqrt{k_\parallel^2 + (\frac{2\pi\vec{U}}{r_\nu})^2}), \tag{3.10}$$

where $C(z) = C'(z)\theta_0^2/2r_\nu^2$.

Bharadwaj et al. (2001) considered the visibility correlation at nearby baselines to estimate the H I power spectrum from the observed visibilities. The nearby baseline correlation reduces the noise bias that appears by correlating the visibilities in the same baselines and introduces the factor $\exp\left(-\frac{|\frac{2\pi}{r_\nu}(\vec{U}-\vec{U'}|^2}{(\frac{2}{r_\nu\theta_0})^2}\right)$. In this Chapter, we do not consider the effect of measurement noise in the visibilities and correlating the visibilities at the

same baselines. Furthermore, the visibility correlation is also done at the same frequencies. Hence eqn (3.10) simplifies to

$$V_{2L}(\vec{U},\nu) = C(z)|S_L(\vec{U},z_s,z_L)|^2 \int dk_{\parallel} P_{HI}(\sqrt{k_{\parallel}^2 + (\frac{2\pi\vec{U}}{r_\nu})^2}). \tag{3.11}$$

Clearly, the effect of gravitational lensing is a magnification of the visibility correlation by a factor of $\mid S_L \mid^2$.

3.2 Simulating lensed 21 cm power spectrum

In this section, we discuss the methodology to simulate lensed 21 cm power spectrum from the post reionization universe. We use four simple models for the lensing potential based on strong lensing by galaxy clusters and calculate the corresponding lensing sampling functions.

3.2.1 Model for Lensing Potential

Strong lensing by galaxy clusters is studied very widely in literature (Jauzac et al., 2015; Limousin et al., 2008; Richard et al., 2010a, 2007) where multiple images of lensed galaxies are used to reconstruct the gravitational potential of the lens. Many different approaches to model the projected lensing potential exist. Barkana (1998) use a Soften Power-law Elliptical Potential (SPEP) model to develop a computational algorithm for estimating the lensing potential. A semi-analytical model of dark matter halo with different profiles like NFW (Li and Ostriker, 2002), soften and singular isothermal potential are discussed in Li and Ostriker (2002). The basic idea behind the reconstruction of the lensing potential in most of the methods is to start with a parametric model of the lensing potential and reconstruct the source structure given the lensed images (Killedar et al., 2012). The parameter of the model is then tuned, mostly using an MCMC variant, to find the best

approximation to the lensing potential (Birrer et al., 2015; Jullo et al., 2007). A typical cluster potential has several components, one or two large dark matter halos along with smaller components arising from the gravitational potential of the cluster galaxies. The larger halos, however, are the most important elements for the overall lensing (Elíasdóttir et al., 2007). Kassiola and Kovner (1993) have used the Pseudo Isothermal Elliptical Mass Distribution (PIEMD) to model the individual cluster potentials. The PIEMD model is one of the widely used parametric models for the dark matter halo potentials of the galaxy clusters.

The projected potential for the PIEMD can be written as a function of the angular coordinates from the centre of the field of view of observations as

$$\begin{aligned} \psi(\theta_x,\theta_y) &= 6\pi\frac{D_{ds}}{D_s}\frac{\theta_s+\theta_a}{\theta_s}\frac{\sigma_v^2}{c^2}\,f(\theta), \\ f(\theta) &= \sqrt{\theta_s^2+\theta^2}-\sqrt{\theta_a^2+\theta^2}+\theta_a\ln\left(\theta_a+\sqrt{\theta_a^2+\theta^2}\right)-\theta_s\ln\left(\theta_s+\sqrt{\theta_s^2+\theta^2}\right), \end{aligned} \tag{3.12}$$

where D_{ds} and D_s are the distance between lens and source and the source and the observers respectively. The parameters θ_s and θ_a are the cut and the core radius, σ_v gives the dark matter velocity dispersion to gravitationally support the halo. The angular variable θ depends on the angular coordinates θ_x and θ_y as

$$\theta^2=\left[\frac{(\theta_x-\theta_{0x})\cos\chi+(\theta_y-\theta_{0y})\sin\chi}{1+\varepsilon}\right]^2+\left[\frac{-(\theta_x-\theta_{0x})\sin\chi+(\theta_y-\theta_{0y})\cos\chi}{1-\varepsilon}\right]^2, \tag{3.13}$$

where ε is the ellipticity of the halo and χ gives the position angle of the ellipse. Each of the PIEMD components in the dark matter halo of the galaxy cluster is defined by seven parameters.

Here, we consider four models of the cluster potentials based on PIEMD parametrization. The parameters for the models are given in Table 4.1 and estimated in accordance with Cerny (2018); Johnson et al. (2014); Smith et al. (2005). Though these choices of

parameters do not reflect any particular observed galaxy cluster, the parameters are chosen to lie within the known ranges of the observed galaxy clusters. Here is a brief description of the four models we choose here:

- **M 1**: A single circular pseudo isothermal halo.
- **M 2**: A single elliptical pseudo isothermal halo.
- **M 3**: Two component PIEMD cluster halo with the same parameters except for the position of their centres.
- **M 4**: Two component PIEMD cluster halo with different parameters for the components.

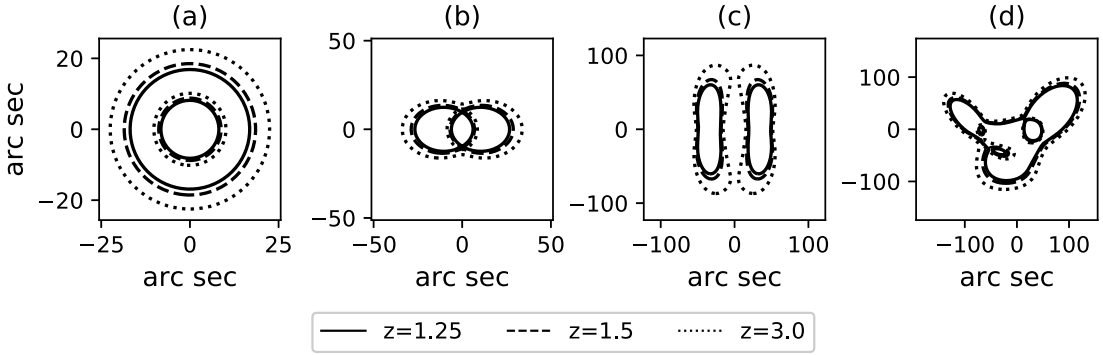

Figure 3.1: Critical curves generated by the four lensing models at the fiducial source redshifts of $1.25, 1.5$ and 3.0.

The gravitational lens at a redshift z_L only modifies the specific intensity from redshifts $z > z_L$. Here, we are considering that all our lens models are at a redshift of 0.3 and $z_L = 1.0$. We first discuss the result with $z_L = 0.3$ in the next section.

Models	x_0 ($'$)	y_0 ($'$)	ε	χ ($^\circ$)	θ_a ($'$)	θ_s ($'$)	σ_v (km sec^{-1})
M 1	0	0	0	0	10	500	1000
M 2	0	0	0.1	0	10	500	1000
M 3	-35	0	0.25	90	20	500	1100
	35	0	0.25	90	20	500	1100
M 4	-50	0	0.30	45	10	500	1000
	50	0	0.2	135	10	500	1500

Table 3.1: Parameters of the PIEMD potential for the four lens models considered in this work.

3.2.2 Point spread function of the gravitational lens

Given a projected lensing potential $\psi(\theta_x, \theta_y)$, the matrix $A_{ij}(\theta_x, \theta_y)$ can be estimated at each angular position as

$$A_{ij}(\theta_x, \theta_y) = \delta_{ij} - \frac{\partial^2 \psi}{\partial \theta_i \partial \theta_j}, \tag{3.14}$$

where (i, j) corresponds to the combinations $(x,x), (x,y), (y,x), (y,y)$ etc, $\delta_{ij} = 1$, if $i = j$ or 0 otherwise. The lensing magnification function $\mu(\theta_x, \theta_y)$ can be calculated as the inverse modulus of the determinant of the matrix A_{ij}. Loutsenko (2018) shows that the lensing magnification function can be approximated as the point spread function of the gravitational lens when the dimension of the lensing potential is much larger than the wavelength of the lensed radiation and interference effects can be neglected. Hence, we may write,

$$G_L(\theta_x, \theta_y) = \frac{1}{det \mid A_{ij}(\theta_x, \theta_y) \mid}. \tag{3.15}$$

We generate a grid in the image plane to estimate the magnification function and hence the point spread function. We show the critical curve for a lens redshift of 0.3 and three different source redshifts for our four lens models in Fig 4.1. The critical curves for the circular model are circular. As the lensing models get complicated the critical curves also show interesting features.

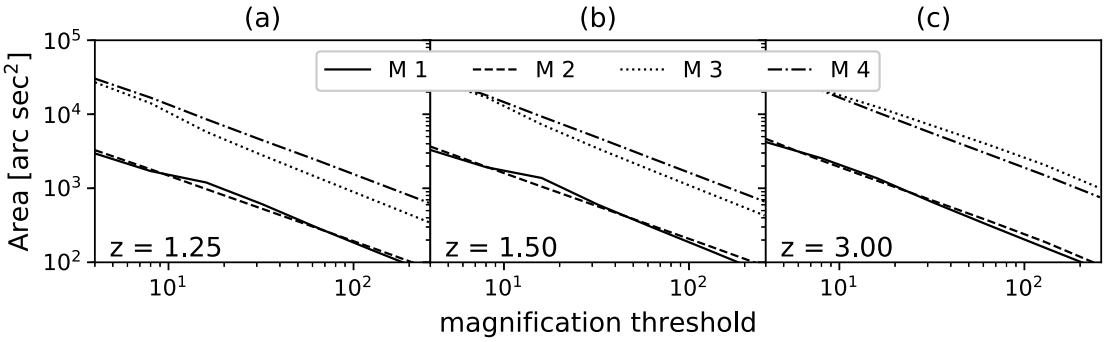

Figure 3.2: Area in arcsec^2 with magnification over a certain threshold is plotted. Each panel shows for all four potentials with the panels (a), (b) and (c) corresponding to source redshift of $1.25, 1.5$ and 3.0 respectively. The lens redshift is 0.3.

The magnification function of the strong gravitational lens is expected to be unity away from the critical curves. Near to the critical curve the magnification increases. An important aspect of the lensing models is the area in the image plane over which the magnification function has a value above a certain threshold (Saini et al., 2001). We plot this area in arcsec^2 as a function of the magnification threshold in Fig 3.2. In each panel, we show results from four models with different panels corresponding to different source redshifts. Lens redshift is kept fixed at $z_L = 0.3$. Clearly, the single halo models have significantly lower magnifications compared to the double halo models. The area for a given model increases slowly with the redshifts. Within the two single and two double halo model we do not notice much difference in the effectiveness of the magnification reflected in these plots.

3.3 Results

We calculate the Fourier transform of G_L and estimate the modulus square of the azimuth averaged lensing sampling function $\mid S_L \mid^2$. Each panel of Fig 3.3 shows the variation of $\mid S_L \mid^2$ with baselines for all four lens models for $z_L = 0.3$. Note that the point spread function of the gravitational lens and hence the lensing sampling function depends on both

the source and the lens redshifts. Three panels (a), (b) and (c) corresponds to the three different source redshifts.

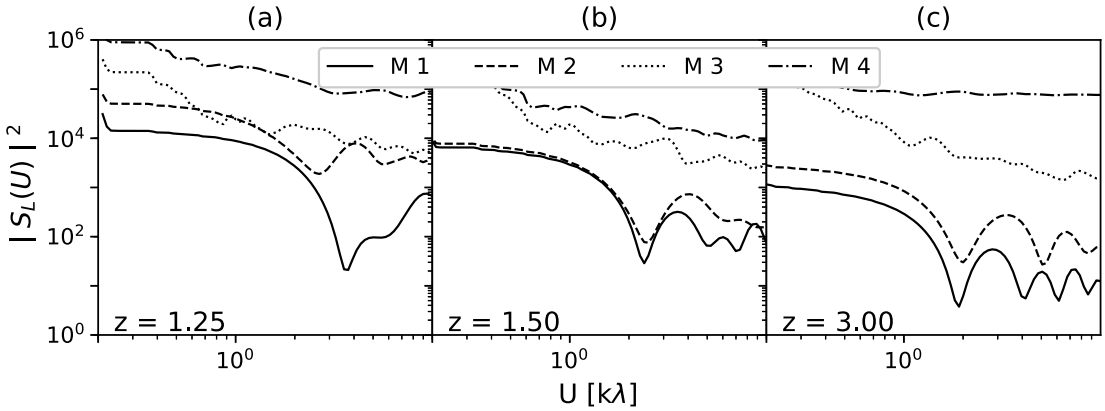

Figure 3.3: Modulus square of the azimuthally averaged lensing sampling function is plotted against baselines. Each panel shows for all four potential with the panels (a), (b) and (c) corresponding to source redshift of 1.25, 1.5 and 3.0 respectively. The lens redshift is 0.3.

The sharp increase of the magnification function near to the critical curves results in oscillation in the sampling function and can be seen clearly in all models at larger baselines. The single halo models (M 1 and M 2) show the almost constant value of the $\mid S_L \mid^2$ at baselines corresponding to the Einstein radius of each model and then a sharp decrease. At higher baselines, the single halo models have strong oscillatory features. The double halo models, in general, have higher values of $\mid S_L \mid^2$ compared to the single halo models. This is expected from the Fig 3.2 where the same models show a significantly large portion of the area over a certain high magnification threshold. The oscillations in the double halo models are also subdominant because their corresponding magnification function has larger values at different places in the image planes.

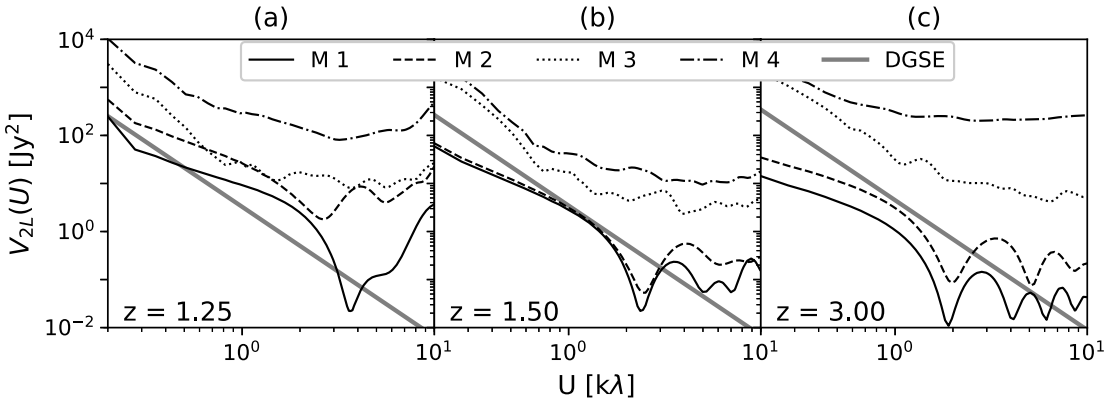

Figure 3.4: Visibility correlation in the presence of strong gravitational lensing is shown as a function of baseline. Each panel shows for all four potentials with the panels (a), (b) and (c) corresponding to source redshift of $1.25, 1.5$ and 3.0 respectively. The grey line corresponds to the expected diffused galactic synchrotron emission (DGSE) from Trott (2016). The lens redshift is 0.3.

We use the eqn (3.11) to estimate the lensed visibility correlation for our four lens models. The azimuthally averaged visibility correlation in the presence of the four lens models are shown in Fig 3.4 for the lenses at a redshift of 0.3. Different panels (a), (b) and (c) shows the results for three different redshifts 1.25, 2.5 and 3.0 of the source 21 cm emission. The one halo models show the characteristics oscillations as in Fig 3.3 and have in general lower amplitude than the two halo models. The lensed visibility correlation for the two halo models is over ~ 100 mJy^2 for all the baseline ranges plotted here. They show lesser oscillations as expected and explained earlier. A major challenge in detecting the redshifted H I emission is the presence of strong foreground. The foreground contribution comes from the diffused galactic synchrotron emission (DGSE) as well as the extragalactic compact sources (Jelić et al., 2008; Ram Marthi et al., 2017; Trott, 2016). Though there have been techniques to model and subtract the effect of compact source foregrounds in literature (Choudhuri et al., 2017), mitigating the DGSE is an outstanding challenge towards the detection of the redshifted H I emission. A major advantage of using the strong gravitational lensing to enhance the redshifted H I signal is that the enhancement happens

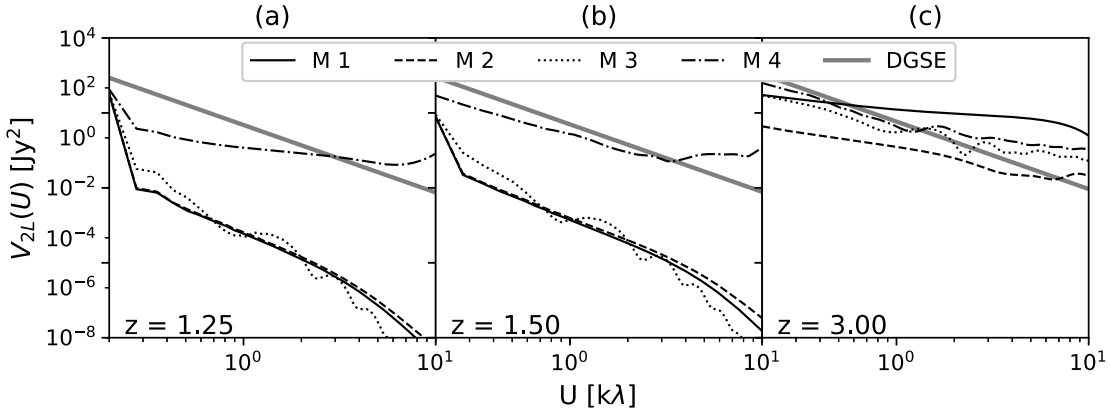

Figure 3.5: Visibility correlation in the presence of strong gravitational lensing is shown as a function of baseline. Each panel shows for all four potentials with the panels (a), (b) and (c) corresponding to source redshift of $1.25, 1.5$ and 3.0 respectively. The grey line corresponds to the expected diffused galactic synchrotron emission (DGSE) from Trott (2016). The lens redshift is 1.0.

only for the H I signal and not for the DGSE. The grey solid lines in the three panels in Fig 3.4 show the DGSE contributions at the frequencies corresponding to the redshifted H I signal (Trott, 2016). We observe that with the two halo models, at least for a baseline range of investigation, the strong lensing enhances the H I signal significantly over the synchrotron foreground.

All the results presented so far are for the lens redshift of $z_L = 0.3$. To investigate the effect of lens redshift, we calculate the visibility correlations in the presence of strong lenses at a redshift of 1.0 in Fig 3.5. All the other parameters of the models including the lenses are kept same. Clearly, in this case, the enhancement of the visibility correlation due to strong lensing for all the model is rather less. In most of the cases, the enhanced H I signal is below the foreground emission.

3.4 Discussion and Conclusion

- In this chapter, we develop a formalism to calculate the power spectrum of the redshifted 21 cm signal using strong gravitational lensing. Using the visibility

correlation to measure the power spectrum, we showed how the lensing sampling function enhances the visibility correlation signal.

- We chose four simple fiducial models of gravitational lenses to demonstrate the effect of strong lensing and the expected visibility correlation signal for lens redshifts of 0.3 and 1.0 and for signal redshifts of 1.25, 1.5 and 3.0.

- We saw that for the lenses at a redshift of 0.3 the visibility correlation signal is significantly magnified at the smaller baselines and hence the large angular scales. At large baselines, the lensed visibility correlation for single halo models showed a sharp drop in signal and became oscillatory in nature.

- For two double halo models that we used here, showed higher enhancement of the visibility correlation.

- We saw that for the lenses at a redshift of 1.0 the enhancement due to gravitational lensing is found to be less significant, limiting the effectiveness of this formalism for cluster lenses at higher redshifts. However, it is to be noted that the enhancement of the visibility correlation signal is quite significant at all the baselines. Hence, even for the range of baseline where the lensed signal is less than the DGSE, the method presented here would help in subtraction of the continuum of DGSE signal.

- A striking advantage of this approach is that the strong lensing by a lens at a redshift of z_L enhances the signal from the redshifted 21 cm emission at a redshift of $z_s > z_L$, however, it does not enhance the diffused emission from the Galaxy, which acts as a foreground to the 21 cm signal.

- The method presented here assumes that the gravitational lens models are already established via certain observations. In fact, using multiple lensing as seen in optical wavelengths, a fairly accurate model for the gravitational lens potential can

be obtained and has been at the forefront of gravitational lens studies in the last few decades. Interested readers can see (Kneib et al. (2011); Suyu et al. (2017)). However, it is to be noted that the lens estimator we are to propose here, requires much better lens models. With the advent of next-generation telescopes, we expect to achieve the lensing models to the required accuracy in the near future.